

Synthesis and Identification of Two Dyes Derived from p-amino phenol and Study of their Effectiveness as Corrosion Inhibitors: Experimental and Theoretical Analysis.

Aseel F. Abdullah , Sura H. Kathim , Athra G. Sager* , Jawad Kadhim Abaies 

Department of Chemistry, College of Science, University of Wasit, Kut, Iraq.

*Corresponding author.

Received 13/10/2023, Revised 27/01/2024, Accepted 29/01/2024, Published Online First 20/11/2024



© 2022 The Author(s). Published by College of Science for Women, University of Baghdad.

This is an Open Access article distributed under the terms of the [Creative Commons Attribution 4.0 International License](https://creativecommons.org/licenses/by/4.0/), which permits unrestricted use, distribution, and reproduction in any medium, provided the original work is properly cited.

Abstract

In this research, two dyes of p-amino phenol were synthesized by reacting the diazonium salt of p-amino phenol with aromatic compounds, including 1-naphthol and p-amino phenol. The new dyes (a and b) were identified by FT-IR, ¹H-NMR, and measurements of some physical properties. The inhibitory activity of the prepared azo compounds against corrosion of carbon steel type C45 in HCl (0.1 M) medium was investigated experimentally by electrochemical measurements. The quantum mechanical method was used to calculate the geometrical structure and physical properties using the Gaussian 09 W program and the density functional theory (DFT) of B3LYP at the 6-311+G (2d, 2p) level. The DFT was utilized for the calculation of inhibition efficiency parameters for dyes that were at equilibrium geometry in vacuum media. The resulting theoretical data revealed that the optimum corrosion inhibitor was compound a.

Keywords: Azo, Corrosion inhibitor, Density functional theory, Electro chemistry, Mullikan charges.

Introduction

Nowadays, compound dyes make up the major group of organic dyes in use. They are highly important materials that are used as coloring agents in the textile, paper, food, and cosmetics industries. In recent years, azo-dyes applications have contributed to the development of various technologies such as liquid crystals, organic photoconductors, and non-linear optics¹⁻³. Through providing a strongly chromophoric label, azo-dyes served as important analytical tools in colorimetric, spectrophotometric, and spectrofluorimetric methods. This property is important to determine the concentration. Also, azo-dyes are important analytical compounds as they are utilized as pH and complexometric indicators and pre-concentration reagents. In terms of pharmacological, azo-dyes compounds were demonstrated that they have several bioactivities such as antibacterial, antifungal, pesticidal, antiviral, and anti-inflammatory activities⁴⁻⁶.

One of the problems that metals face is corrosion. High costs are spent annually to maintain or protect materials from corrosion. Discovering or emerging approaches to inhibit corrosion is a challenging task for scientists interested in this field⁷. Mild steel amongst the rest of the minerals, has drawn a lot of attention as it is utilized in different fields of the mineral industry, especially in construction. The reason behind that is the fascinating property of mild steel and its relatively low-cost industry. This important material is an iron alloy. In acidic media, mild steel easily corrodes, which is considered the main drawback of this important metal. Various industrial processes including acid pickling, acid cleaning, acid descaling, and oil-wet cleaning as well as chemical laboratories considerably depend on the use of acidic solutions^{8,9}. Protection or inhibiting metal corrosion can be attained by different methods. The main practical one is through the use of substances called inhibitors, particularly in acidic

media¹⁰. Economic costs, availability, inhibition efficiency and pollution are the conditions that govern the choice of inhibitors. Therefore, organic materials with N, O and/or S atoms are considered the best inhibitors for mild steel corrosion in acidic media^{11,12}. Adsorption of the inhibitor by the metallic surface results in the formation of an adsorbed inhibitor layer, and subsequently the occurrence of the inhibition process. The chemical features and the structures of this adsorbed layer largely effect on the inhibitors' efficacy at specific experimental circumstances^{13,14}. The present study aims to prepare new two azo-dyes of p-amino phenol

Materials and Methods

All chemicals were acquired from Merck, HIMEDIA and BDH companies and they were used without any purification. *Gallenkamp*, an electro-thermal melting point apparatus was utilized to measure the melting points of compounds a and b. FI-IR spectra were recorded using 8400s-Fourier transitions, Infrared-Spectrometer-Shimadzu, Japan, the disc of KBr in the range of (4000-400) cm^{-1} . ¹H-NMR spectra of the compounds (a and b) were recorded using Bruker, Ultra-shield (500 MHz) NMR spectrometer at the University of Tehran, Iran. A corrosion cell made of Pyrex with (250ml) capacity Consists of two vessels University of Baghdad, Iraq.

Preparation of azo dyes

Preparation of Diazonium Salt

p-amino phenol (0.54 g, 5 mmol) was dissolved in a mixture of (2 mL) of concentrated HCl and (5 mL) distilled water. The obtained solution was then cooled using the ice bath at 0-5 °C before a solution of sodium nitro (NaNO₂) (0.34g, 5 mmol) in water (5 mL) was added drop by drop. The produced mixture was stirred for (10 min) and kept temperature at 4°C. The resulting diazonium salt has been retained from the interaction for the next step (coupling reaction)¹⁴.

General procedure for the coupling a or b compounds with phenols

α -naphthol (5 mmol) was added to 10% NaOH solution (6 ml) and cooled to 0-5 °C. The mixture was added drop by drop to the solution of diazonium chloride defined above with stirring. The produced mixture was left stirring for extra 1 h at 0-5 °C¹⁵. The formed colored compound was collected, washed with cooled water before it was dried at 70 °C. This step is repeated with compound 4-amino

and investigate their application as corrosion inhibitors via using the corrosion cell and three electrodes. the density functional theory (DFT) uses theoretical Analysis to describe the structural nature of dyes through a basis set of (B3LYP) with a 6-311+G (p, d) The theoretical corrosion inhibition parameters such as the energy of the highest occupied molecular orbital and energy of the lowest unoccupied molecular orbital, energy gap electronegativity (χ), electron affinity, global hardness, softness, ionization energy, global electrophilicity, were used for investigating and clarifying the inhibition efficiency of dyes.

phenol. Table 1 displays the physical properties and spectroscopic measurements data of compounds (a and b).

The measurement of the corrosion

To set up the regulator voltage, a host computer and a thermostat were used. Magnetic stirrer, (EmStat 4s, Palm Sens, Holland) potential, and a galvanostat were also utilized. The corrosion is measured by a Pyrex cell consists of internal and external vessels. Size of the cell size was 250 ml, and it consists of three electrodes. The working electrode was the carbon steel, which utilized to measure the potential depending on a reference electrode.

The auxiliary electrode is made of platinum (10 cm), whereas the reference electrode is saturated calomel (Hg/Hg₂Cl₂ sat. KCl). To create and establish a steady-state open circuit potential (E_{ocp}), the working electrode was immersed in a test solution for 15 minutes. Then, in a potential range of ± 200 mV, the electrochemical measurements were performed. The tests of compounds (a and b) were carried out at 298K using a cooling-heating circulating water bath. Fig. 1 shows the corrosion cell and the three electrodes. Proper dimensions of Carbon steel coupons were prepared and utilized for the standard proceedings of the corrosion evaluations. 0.1 M HCl aqueous solution was prepared as an artificial attack medium. The implemented measurements occurred according to the common corrosion procedures of steel specimens after a recorded period of immersion in an environment under the influence of dye inhibitors at definite concentrations (25 and 50 ppm). Table 1 shows the chemical composition of carbon steel C45.

Table 1. Chemical composition of carbon steel C45.

metal	C%	Si%	Mn%	S%	P%	Cu%	Ni%	Cr%	Fe%
Carbon	0.36-0.42	0.15-0.30	1.00-1.40	0.05	0.05	0.50	0.20	0.20	96.88
Steel 45									-97.49

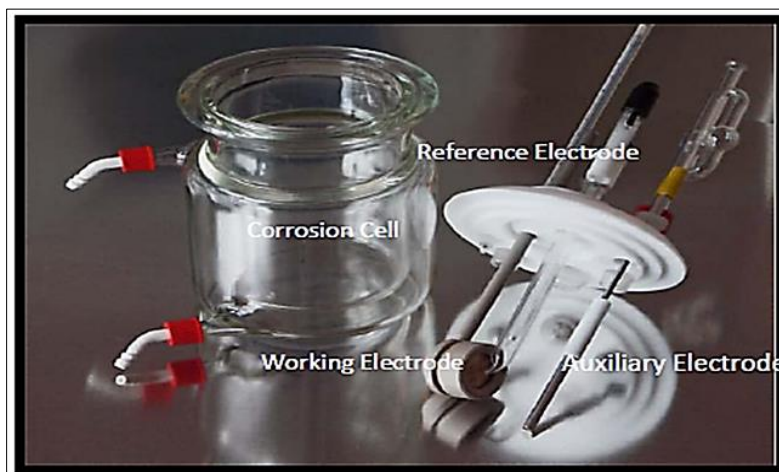
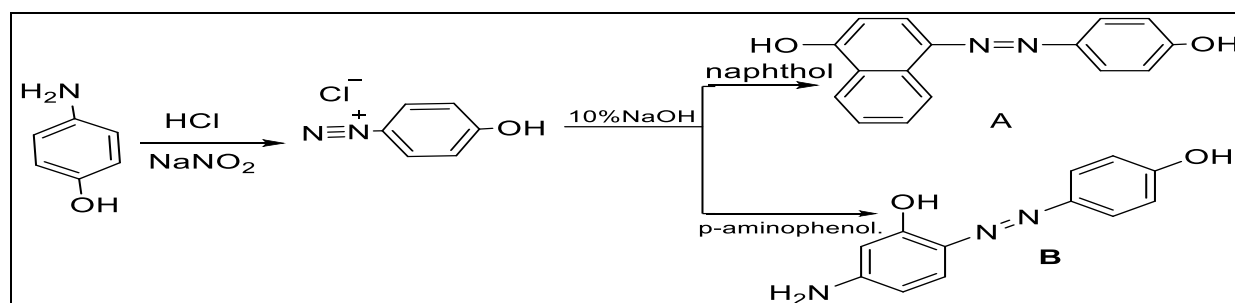


Figure 1. Set up the corrosion cell and three electrodes.

Results and discussion

The reaction of the organic compounds, a diazonium salt and a binding factor produced an azo dye. A diazonium salt (as an electrophile) was subjected to a coupling reaction with an electron-rich compound

including α -naphthol and 4-aminophenol. Diazotization and coupling procedures were employed to synthesize azo dyes derived from 4-aminophenol¹⁴⁻¹⁶. Scheme 1 illustrates the synthesis of azo derivatives a and b.



Scheme 1. Preparation route of the compounds a and b .

The FT-IR spectra of 4-aminophenol, Fig. 2 shows two characteristic absorption bands at 3340 cm^{-1} and 3278 cm^{-1} which are attributed to νNH_2 and νOH groups respectively, 3005-3178 cm^{-1} of $\nu\text{C-H}$ aromatic and 1612 cm^{-1} of $\nu\text{C=C}$ aromatic¹⁷. FT-IR measurements data of azo derivatives (a and b) are exhibited in Table 2. FT-IR data of compound [a] are displayed in Fig. 3. It is clearly can be seen the appearance of νOH at (3367) cm^{-1} and $\nu(\text{N}=\text{N})$ stretching bands at (1454) cm^{-1} ¹⁸. Fig. 4 showed FT-IR bands of compound [b]. This figure displayed the presence of the asymmetric and symmetric

stretching bands of $\nu(\text{NH}_2)$ absorption at 3425 cm^{-1} asym.; 3344 cm^{-1} sym. Fig. 3 also exhibited the existence of the $\nu(\text{N}=\text{N})$ stretching at 1454 cm^{-1} . $^1\text{H-NMR}$ spectrum of compound (a) is shown in Fig. 5. The spectrum exhibited the following characteristic signals $\delta(\text{ppm})$: 6.86-8.24(m, 7H, Ar-H); 10.13(s, 1H, OH). $^1\text{H-NMR}$ spectrum of compound (b) is displayed in Fig. 6. This spectrum exhibited the following characteristic signals $\delta(\text{ppm})$: 5.11(s, 2H, NH_2); 6.34-8.27(m, 10H, Ar-H); 10.03(s, 1H, OH). $^1\text{H-NMR}$ data of compounds (a and b) are shown Table 3.

Table 2. Physical properties and FT-IR spectral data of azo compounds a and b.

No.	Physical properties					FTIR /Major Absorption (cm ⁻¹)				
	M.P	MWt (g/mol)	Molecular structure	color	Yield %	$\nu(\text{NH}_2)$	$\nu(\text{OH})$	$\nu(\text{C-H})$ Ar	$\nu(\text{C=C})$ Ar.	$\nu(\text{N=N})$
a	100-102	264.28	C ₁₆ H ₂₂ N ₂ O ₂	Dark Red	65	-	3367	3051	1597	1454
b	107-105	229.22	C ₁₂ H ₁₁ N ₃ O ₂	Orange	74	3425	3344	3024	1590	1454

Table 3. ¹H-NMR spectral data of compounds a and b.

No.	Compound structure	¹ H-NMR spectral data (δppm)
a	(E)-2-((4-hydroxyphenyl) diazenyl) naphthalen-1-ol	6.86-8.24 (m,10H,Ar-H); 10.13 (s,1H,OH, Phenol)
b	(E)-4-amino-2-((4-hydroxyphenyl) diazenyl) phenol	5.11(s,2H,NH ₂);6.20-8.15 (m, 7H, Ar-H);10.03(s,1H,OH, Phenol)

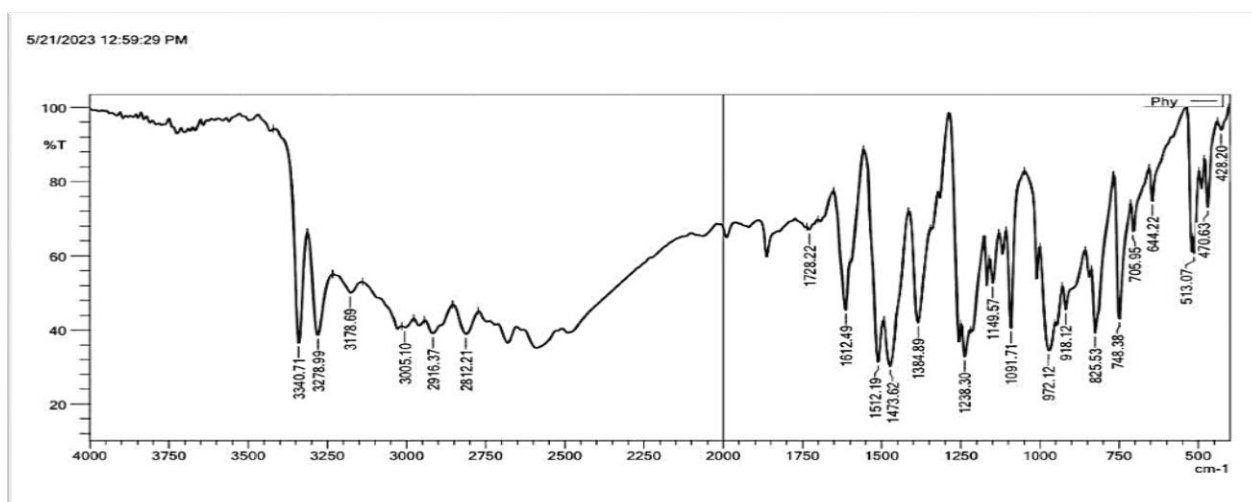


Figure 2. FT-IR spectrum of 4-aminophenol.

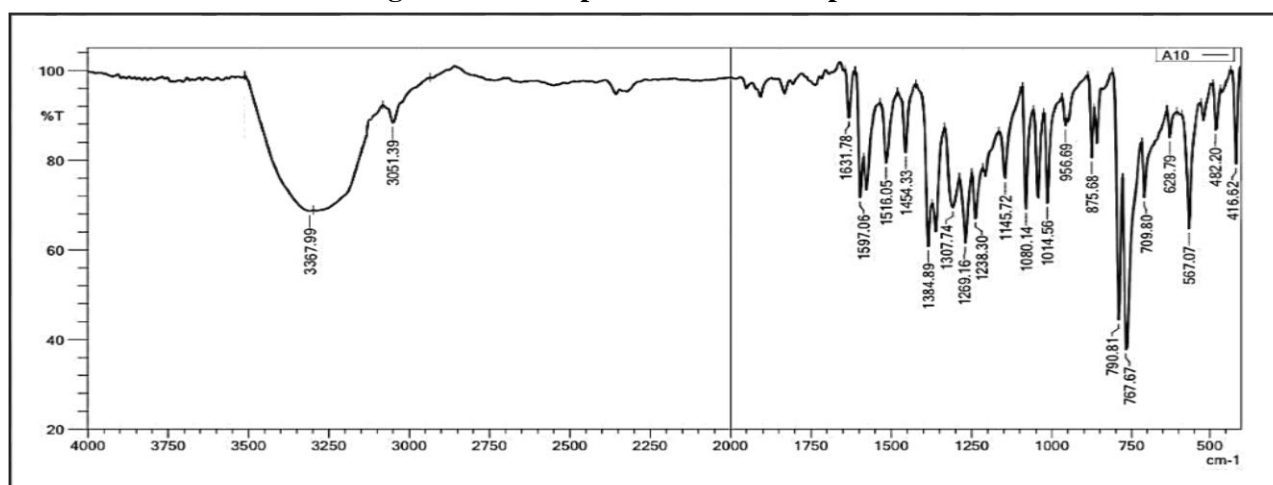


Figure 3. FT-IR spectrum of compound a.

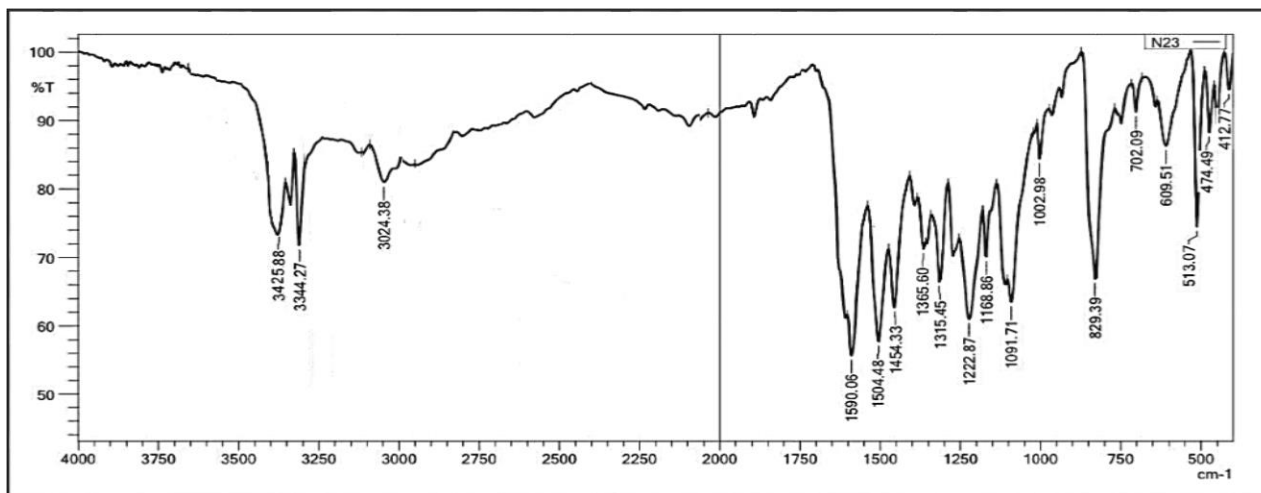


Figure 4. FT-IR spectrum of compound b.

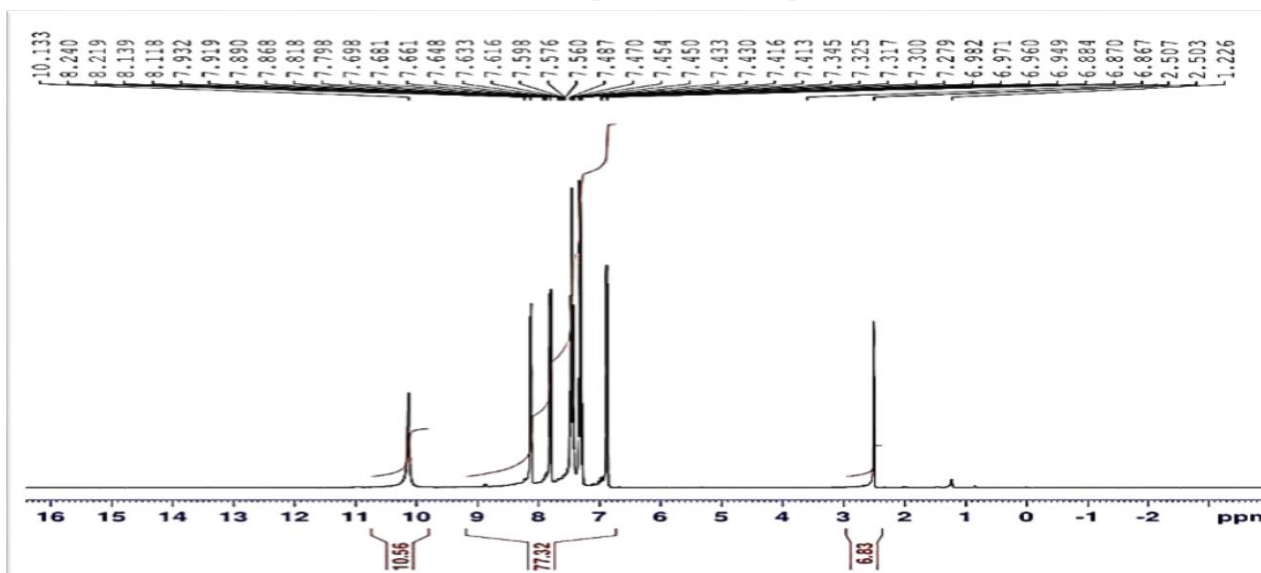


Figure 5. ¹H-NMR spectrum of compound a.

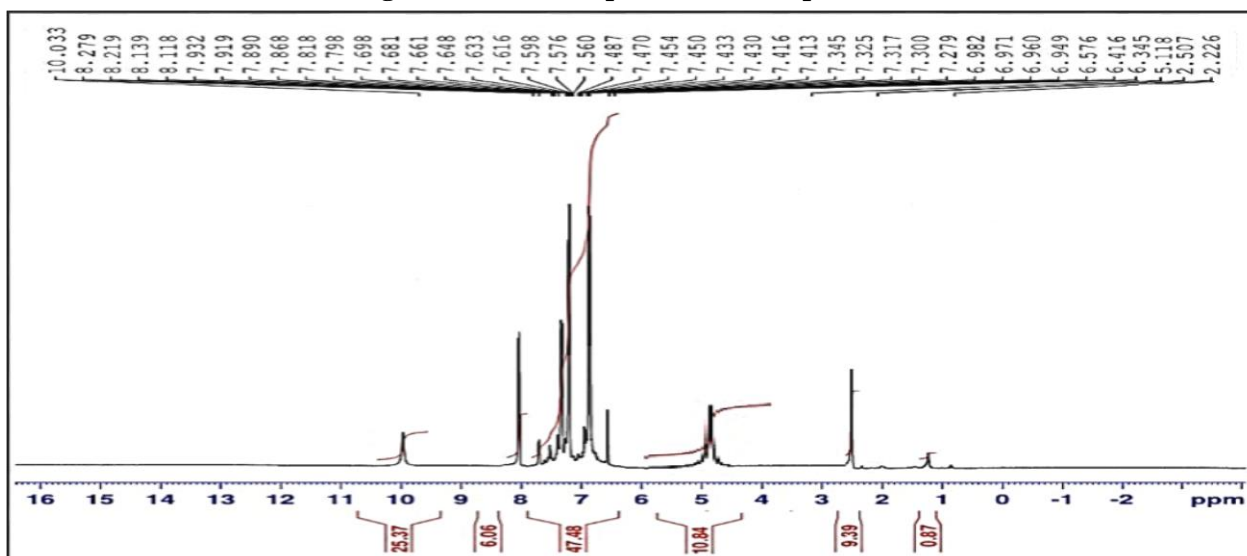


Figure 6. ¹H-NMR spectrum for compound b.

The Quantum chemical calculations of the compounds a and b.

The density functional theory (DFT) was used to describe the structural nature of dyes through basis set of (B3LYP) with a 6-311+G (p, d)^{19,20}. The theoretical corrosion inhibition parameters such as "energy of the highest occupied molecular orbital (EHOMO) and energy of the lowest unoccupied molecular orbital (ELUMO), energy gap (ΔE) between EHOMO and ELUMO, dipole moment (μ), electronegativity (χ), electron affinity (A), global hardness (η), softness (σ), ionization energy (IE), global electrophilicity (ω), the fraction of electrons transferred (ΔN) and the total energy (E_{tot})"²¹ were used for investigation and clarifying the inhibition efficiency of compounds. The compounds (a and b) were designed using ChemDraw. ChemDraw program was used to draw the structures compounds. The program (Gaussian 09W) was employed to compute the molecular geometry²². The

corresponding geometry was calculated at a vacuum phase. Fig. 7 shows the atoms numbering of compounds a and b. The bond angles, bond distances, and dihedral angles were computed and investigated as structural parameters of compounds a and b as shown in Table 4.

Length bond was observed of compound (a) for C8-C9 (1.39164Å). The shortest bond length was observed for O11H27(0.97133Å). The bond angles were locating between (107.462Å°) for N20N19C14 and (120.02678Å°) for N19C14C15. The dihedral angles values (trans and cis) demonstrated that the compound was not planar and dihedral angles are not 0.0 degrees. While, Table 4 shows the longest bond length that was noticed, which belongs to compound (b) for C22-C26(1.39528Å). The shortest bond length was noticed for N28-H11 (1.0498Å). The bond angles were locating between (107.5044Å°) for O21C22C26 and (120.046Å°) for O21C22C26. The dihedral angles values (trans and cis) demonstrated that the compound was not planar.

Table 4. The bond length, distances, and dihedral angles for compounds a and b in media of vacuum as calculated by using DFT method.

Description Bond length	Bond length (Å)	Description angle (deg)	Angle (deg)	Description Dihedral Angle (deg)	Dihedral angle (deg)
Compound a					
N20N19	1.24861	N20N19C14	107.46128	C14N20N19C27	179.94297
O11C10	1.35525	O11C10C9	119.61113	O11C10C5C4	179.97257
O18C17	1.35474	O18C17C16	119.99817	O18C17C12C13	-179.98368
N20C7	1.26032	N20C7C4	119.63226	N20C7C4C5	179.97646
N19C14	1.25991	N19C14C15	120.02678	C14N19N20C7	179.94297
O11H27	0.97133	H27O11C10	107.98579	H27O11C10C9	179.97226
O18H32	0.97168	H32O18C17	108.03875	H32O18C17C16	-179.93969
C8C9	1.39164	C8C9C10	119.97430	C8C9C10O11	-179.97312
C15H30	1.09966	H30C15C14	120.02140	H30C15C14C13	-179.96757
Compound b					
N28C27	1.26659	N28C27C26	119.99593	N28C27C26C22	-179.98725
C22 O21	1.35476	O21C22C26	120.04644	O21C22C26C27	-170.98385
N12N13	1.24796	N12N13C18	107.50440	C18N13N12C23	-179.98777
N12C23	1.26072	N12N13C23	107.51378	N12C23C24C25	179.98281
O14C15	1.35450	O14C15C16	120.02373	O14C15C28C19	179.98921
N28H10	1.05094	C27N28H10	119.95978	H10N28C27C25	-179.94175
N28H11	1.04980	C27N28H11	120.04447	H11N28C27C26	-179.99596
C26C22	1.39528	C26C22C23	119.94271	C26C22O21H3	-179.97975

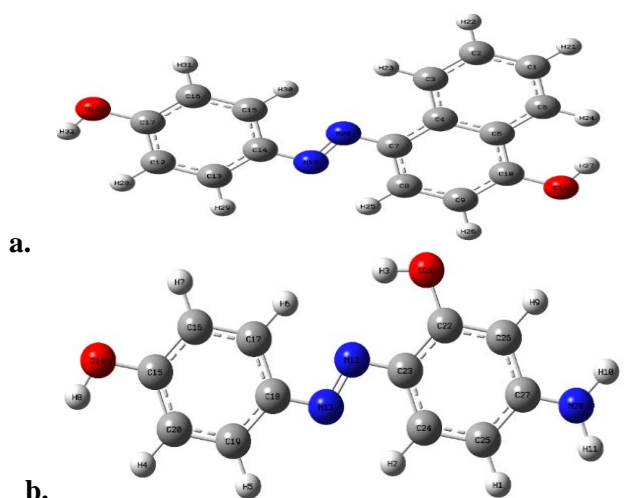


Figure 7. The numbering of atoms of compounds a and b.

Global Reactivity of Molecular

In order to predict the adsorption centers of compounds [a and b], the frontier orbital theory was utilized. The centers of adsorption in compounds a and b will have a significant role in inhibition the reaction of metal surface/ molecule (a and b) ²³.

Tables 5 - 7 show the calculated quantum chemical parameters. The calculation of parameters were carried out using the following vital equations:

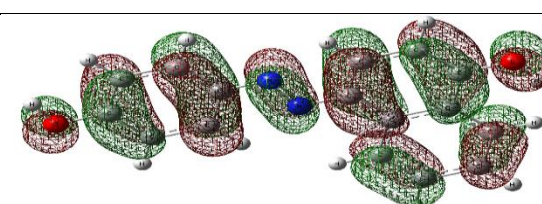
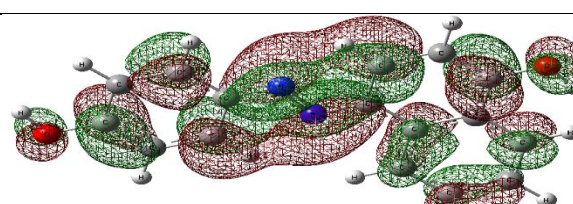
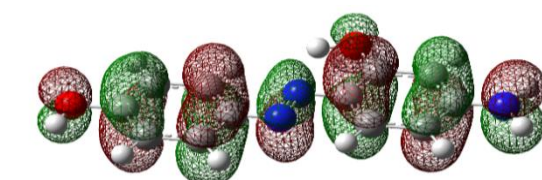
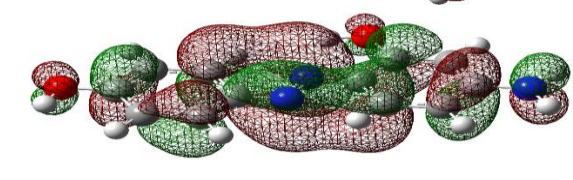
$$\begin{aligned}
 IP &= -EHOMO && \dots \dots 1 \\
 EA &= -ELUMO && \dots \dots 2 \\
 H &= \frac{IE - EA}{2} && \dots \dots 3 \\
 X &= \frac{IE + EA}{2} && \dots \dots 4 \\
 S &= \frac{1}{\eta} && \dots \dots 5 \\
 \omega &= \frac{-X^2}{2\eta} = \frac{\mu^2}{2\eta} && \dots \dots 6
 \end{aligned}$$

Where: IP=Ionization potential; EA= Electron affinity; H =Hardness;

X =Electro negativity, softness = S; the Global electrophilicity index= ω ; the electrons transferred = ΔN .

Table .5 shows the geometry structure of compounds a and b in a vacuum. The geometry structure consists density distributions of HOMO and LUMO. The location of HOMO is mostly on the diazine moiety. Accordingly, the location of the favorite actives sites for the attack by electrophile are in the region that surround N atoms and O atoms. While, LUMO electronic density was distributed around the aromatic ring and surround diazine moiety, which implies the majority of planar region is in the compound molecules.

Table 5. Frontier Molecular Orbital density distributions of compounds a and b.

NO	HOMO D3	LOMO D3
a		
b		

The global chemical reactivity descriptor ($\mu = -\chi$) describes a chemical potential. The chemical potential (μ) measures the escaping of an electron and describes the molecular electronegativity. If (μ) was more negative, the molecule would lose an electron easier. In a comparison with compound a, compound b is less stable and more reactive. Nevertheless, electronegativity of compound a is bigger than that of compound b as illustrated in Table

7. Hardness (η) and softness (S) will be useful concepts in understanding the behavior of atoms. The values of these parameters were theoretically calculated. The calculation data revealed that the compound b possesses the biggest hardness value ($\eta = 1.29$ eV). This implies that the hardest molecule is b. The molecule possesses the biggest softness = 0.82963, which means that it is the softest molecule. The value electrophilicity (ω) gives knowledge about the

stabilization energy become the system becomes rich with electrons that moved from ambient. On the other hand, the molecule b with the slightest values of $\omega = 5.01243$, so the compound (b) is good

nucleophile. While, the molecule a is a good electrophile as it has the highest value of ($\omega = 6.46756$).

Table 6. The some physical properties of the inhibitor molecules a and b at the equilibrium geometry by using DFT Method.

No.	Molecular formula	EHOMO(eV)	ELOMO(eV)	ΔE (eV)	μ (Debye)
a	C ₁₆ H ₂₂ N ₂ O ₂	-5.1539528	-2.743242	2.41071	0.187156
b	C ₁₂ H ₁₁ N ₃ O ₂	-4.8883637	-2.306489	2.58187	4.245720

Table 7. Quantum chemical parameters for inhibitor molecules [a and b] by using DFT Method.

No.	IE (eV)	EA (eV)	η (eV)	μ (eV)	X (eV)	S (eV)	ω (eV)	ΔN (e)	N _{max}	CP
a	5.15395	2.74324	1.205	-3.94	3.9486	0.82963	6.46756	1.26577	3.27588	-3.9486
b	4.88836	2.30649	1.290	-3.59	3.59743	0.77463	5.01243	1.31787	2.78668	-3.5974

Local reactivity descriptors.

Calculating Fukui functions will help researchers to understand the active site of molecules. Chemical reaction depends on a variation in the electrons number, which requires a minimum one electron being added or subtracted in the frontier orbitals.

Fukui functions $f^+_{(r)}$, $f^-_{(r)}$ and $f^0_{(r)}$ are calculated by the following equations:

$$f^+ = [q(N+1) - q(N)] \quad \text{for nucleophilic attack} \quad \dots\dots 7$$

$$f^- = [q(N) - q(N-1)] \quad \text{for electrophilic attack} \quad \dots\dots 8$$

$$f^0 = [q(N+1) - q(N-1)] / 2 \quad \text{for radical attack.} \quad \dots\dots 9$$

Where : $q(N)$ = the charge located on the atom for neutral molecule; $q(N+1)$ = anionic specie, and $(N-1)$ =cationic specie^{23,24}.

The values of descriptors chemical were calculated at level of B3LYP/6-31G (d, p) by Mulliken charges on molecules atoms. For compound a, the greatest preferred susceptible spot for a nucleophilic attack is placed on 18O. Nonetheless, the greatest reactive position for electrophilic attack is placed on 19N. The most preferred reactive spot for a free radical attack is on 19N. Moreover, 14O is the greatest susceptible spot to nucleophilic attack for compound b. Whereas, the greatest susceptible spot for both electrophilic and free radical attacks is on 13N Table 8.

Table 8. Values of the Fukui function of the molecules a and b.

compound	a			b			
	Atom	f^+	f^-	Atom	f^+	f^-	f^0
1c		-0.03179	-0.0311	1H	0.046628	0.046077	0.046353
2C		0.033693	0.048078	2H	0.02935	0.023057	0.026204
3c		0.025342	0.002745	3H	0.010092	0.00471	0.007401
4C		-0.00055	0.02515	4H	0.044667	0.041944	0.043306
5C		0.0073	-0.01149	5H	0.040118	0.036555	0.038337
6C		0.042677	0.040163	6H	0.029109	0.017074	0.023092
7C		0.042619	-0.00319	7H	0.04166	0.041516	0.041588
8C		-0.00025	0.05186	8H	0.023755	0.021577	0.022666
9C		0.016095	-0.00459	9H	0.044667	0.042289	0.043478
10C		0.056801	0.059623	10H	0.041525	0.036862	0.039194
11O		0.071532	0.054533	H11	0.040056	0.033689	0.036873
12C		0.033864	0.03032	12N	0.01719	0.073392	0.045291
13C		0.04155	0.042922	13N	0.05246	<u>0.115838</u>	<u>0.084149</u>
14C		-0.02119	-0.05335	14 O	<u>0.069577</u>	0.042217	0.055897
15C		0.038535	0.077687	15C	0.051462	0.061068	0.056265
16C		0.021152	-0.00517	16C	0.028642	-0.01169	0.008476
17C		0.051751	0.066749	17C	0.021473	0.063209	0.042341
18O		<u>0.064727</u>	0.042648	18C	-0.00898	-0.02794	-0.01846
19N		0.038896	<u>0.108636</u>	19C	0.046861	0.053268	0.050065
20N		0.023712	0.051386	20C	0.041643	0.045354	0.043499



21 H	0.038692	0.03693	0.037811	21O	0.052689	0.046941	0.049815
22 H	0.03627	0.034544	0.035407	22C	0.046207	0.056832	0.05152
23 H	0.019388	0.011125	0.015257	23C	0.046946	-0.00419	0.021379
24 H	0.032347	0.031515	0.031931	24C	0.006671	0.07539	0.041031
25 H	0.031725	0.022378	0.027052	25C	0.019067	-0.04012	-0.01053
26 H	0.042547	0.040136	0.041342	26C	0.006753	-0.0125	-0.00287
27 H	0.018797	0.015929	0.017363	27C	0.059635	0.095435	0.077535
28 H	0.041627	0.039983	0.040805	28N	0.050082	0.02214	0.036111
29H	0.036923	0.035455	0.036189				
30H	0.022104	0.01725	0.019677				
31H	0.037277	0.038064	0.037671				
32H	0.022262	0.020878	0.02157				

Corrosion study

Potentiodynamic polarization curves and corrosion kinetic

Extraction of polarization curves for carbon steel corrosion of the synthesized inhibitors (a and b) was achieved in HCl solution. The extraction of polarization curves was carried out at (25, 50 ppm) concentrations of (a and b) inhibitors and the ambient temperature was 298 Kelvin in the existence and absence of the inhibitors as displayed in Fig. 8. This figure also shows polarization curves for the molecules (a and b) and the blank (HCl solution). The electrochemical corrosion parameters such as corrosion potential (E_{corr}), and corrosion current density (I_{corr}) attained by cathodic and anodic areas of the Tafel lines were described in Table 9.

IE% and Θ were calculated by the following²⁵:

$$\%IE = (I_{corr(uninh)} - I_{corr(inh)} / I_{corr(uninh)}) \times 100 \dots\dots 10$$

$$\Theta = (I_{corr(uninh)} - I_{corr(inh)} / I_{corr(uninh)}) \dots\dots 11$$

Where: $I_{corr(inh)}$ = current densities of inhibited corrosion, $I_{corr(uninh)}$ = uninhibited current densities.

Table 9 illustrates that at a temperature of 298K, the value (IE%) of the molecule (a) is bigger than that of the compound (b). This demonstrates the

physisorption inhibition occurrence. These results disclose that at 25 and 50 ppm concentrations of molecules a and b, the I_{corr} value is reduced, which indicates that these compounds are good inhibitors of corrosion. Moreover, besides increasing the concentration of inhibitors, a minor change in E_{corr} to negative values is caused by molecules a and b, resulting in an improvement in inhibition efficiency. Also, it was found that the highest inhibition efficacy was up to 91%, belonging to compound a with a concentration of 50 ppm and at a temperature of 298K. This is attributed to the existence of groups with high electronic density including phenyl rings, hydroxyl groups, N2 atoms, and Pi bonds, which participate in the generation of coordination links with the metal surface. Accordingly, a preservative layer will be formed on the metal surface in acidic medium, and subsequently prevents carbon steel corrosion.

A study of the temperature effect on efficiency of inhibition was not achieved and it will be applied in a later study. It was suggested that the temperature might increase the mobility of the inhibitor molecules, resulting in a reduction in the contact between the inhibitor molecules and the carbon steel surface.

The inhibitor molecules motion increases as temperature increases.²⁶

Table 9. Corrosion parameters for blank and compounds a and b in (0. 1M) HCl solutions.

Comp	C (ppm)	$E_{corr.}$ vs.SCE (mV)	$I_{corr.}$ (mA cm ⁻²)	$I_{corr./r}$	Resis.	Anodic b_a (mV Dec ⁻¹)	Cathodic $-b_c$ (mV Dec ⁻¹)	Corr. rate,	IE%	Θ
Blank		- 0.527	163.5	3.269E-4	143.2	0.126	0.094	1.605	-	-
a	50	-0.630	15.36	3.073 E-5	2957	0.167	0.279	0.151	91	0.91
	25	-0.637	16.33	266.E-5	2109	0.127	0.213	0.160	90	0.90
b	25	-0.634	28.43	5.685 E-5	1690	0.189	0.276	0.279	83	0.83
	50	-0.638	23.99	5.798E-5	1880	0.175	0.255	-0.618	85	0.85

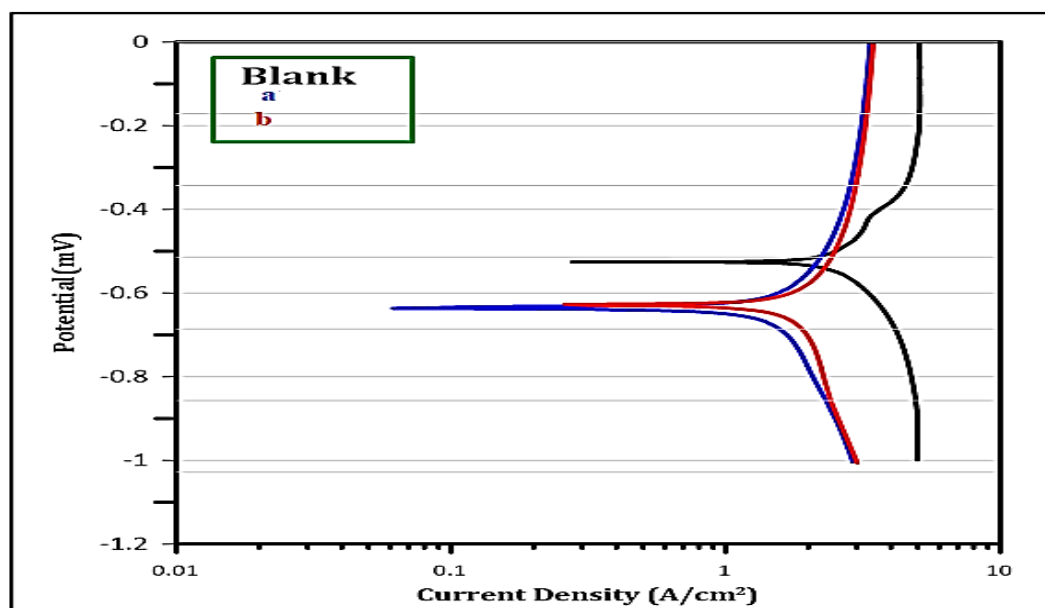


Figure 8. Polarization curves for compound a and b (25 ppm) at 298K.

Conclusion

The values of the theoretical chemical parameters suggest that compound (a) has a greater tendency to interact with the metal surface in a vacuum, and it is a good inhibitor. The results of density functional theory (DFT) were used to describe the structural nature of dyes through a basis set of (B3LYP) with 6-311+G (p, d) calculations on p-amino phenol derivatives that have been presented in a vacuum. The HOMO, LUMO, and charges on atoms predict a

similar center (N=N) that would prefer to be attacked by nucleophilic or electrophilic species. The results of DFT/B3LYP were closer to the experimental data. Experimentally, it was observed that the corrosion of carbon steel C45 in the corrosive medium with compound (a) inhibitor was decreased. Also, compound (a) inhibition efficiency in the HCl solution was (91%).

Acknowledgment

The authors are thankful to the University of Wasit for supporting this research, and the University of

Basra for the help in providing the analysis techniques for our samples.

Author's Declaration

- Conflicts of Interest: None.
- We hereby confirm that all the Figures and Tables in the manuscript are ours. Furthermore, any Figures and images, that are not ours, have been included with the necessary permission for re-publication, which is attached to the manuscript.
- No animal studies are present in the manuscript.
- No human studies are present in the manuscript.
- No potentially identified images or data are present in the manuscript.
- Ethical Clearance: The project was approved by the local ethical committee at University of Waist.

Author's Contribution statements

A.G. S., A. F. A., S.H. K., and J.K.A. contributed to the design and implementation of the research, to the

analysis of the results, and to the writing of the manuscript.

References

1. Kamoon RA, Al-Mudhafar MMJ, Omar TN-A. Synthesis, Characterization and Antimicrobial Evaluation New Azo Compounds Derived from Sulfonamides and Isatin Schiff Base, *Int J Drug Delivery Tech.* 2020; 10(1): 150-155. <http://dx.doi.org/10.25258/ijddt.10.1.22>
2. Ibraheem I H, Mubder N S, Abdullah M A, Al-Neshmi H. Synthesis, characterization and bioactivity Study from azo -ligand derived from methyl-2-amino benzoate with some metal ions. *Baghdad Sci J.* 2023; 20(1): 114-120. <https://doi.org/10.21123/bsj.2022.6584>
3. Benkhaya S, M'rabet S, El Harfi A. Classifications, properties, recent synthesis and applications of azo dyes. *Heliyon.* 2020 Jan 31; 6(1): e03271. <https://doi.org/10.1016/j.heliyon.2020.e03271>
4. Mezgebe K, Mulugeta E. Synthesis and pharmacological activities of azo dye derivatives incorporating heterocyclic scaffolds: a review. *RSC Adv.* 2022 Sep 13; 12(40): 25932-25946. <https://doi.org/10.1039/d2ra04934a>
5. Tahir T, Ashfaq M, Saleem M, Rafiq M, Shahzad MI, Kotwica-Mojzycz K, et al. Pyridine Scaffolds, Phenols and Derivatives of Azo Moiety: Current Therapeutic Perspectives. *Molecules.* 2021 Aug 11; 26(16): 4872-4828. <https://doi.org/10.3390/molecules26164872>
6. Al-Khuzai MGAn, Al-Majidi SMH. Synthesis and characterization of new azo compounds linked to 1,8-naphthalimide as new fluorescent dispersed dyes for cotton fibers. *AIP Conf Proc.* 2020; 2290: 030011. <https://doi.org/10.1063/5.0027354>
7. Aftan MM, Toma MA, Dalaf AH, Kaain, H. Synthesis and Characterization of New Azo Dyes Based on Thiazole and Assess the Biological and Laser Efficacy for Them and Study their Dyeing Application. *Egypt J Chem.* 2021;64(6): 2903-2911. <https://doi.org/10.21608/ejchem.2021.55296.3163>
8. Kmal RQ, Mohamed AM, Aljeboree AM, Jasim LS, Alkaim AF. Synthesis and Identification of Azo Disperse Dye Derived from 4-Aminoantipyrine and Their Applications to Determine Some Drugs. *Int J Drug Delivery,* 2021; 11(3): 1040-1044. <https://doi.org/10.25258/ijddt.11.3.67>
9. Franco JH, da Silva BF, Dias EFG, de Castro AA, Ramalho TC, Zanoni MVB. Influence of auxochrome group in disperse dyes bearing azo groups as chromophore center in the biotransformation and molecular docking prediction by reductase enzyme: Implications and assessment for environmental toxicity of xenobiotics. *Ecotoxicol Environ Saf.* 2018 Sep 30; 160: 114-126. <https://doi.org/10.1016/j.ecoenv.2018.04.066>
10. Zobeidi A, Neghmouche Nacer S, Atia S, Kribaa L, Kerassa A, Kamarchou A, et al. Corrosion Inhibition of Azo Compounds Derived from Schiff Bases on Mild Steel (XC70) in (HCl, 1 M DMSO) Medium: An Experimental and Theoretical Study. *ACS Omega.* 2023 Jun 5; 8(24): 21571-21584. <https://doi.org/10.1021/acsomega.3c00741>
11. Lessa RCdS. Synthetic Organic Molecules as Metallic Corrosion Inhibitors: General Aspects and Trends. *Organics.* 2023; 4(2): 232-250. <https://doi.org/10.3390/org4020019>
12. Khudhair NA, Kadhim MM, Khadom AA. Effect of Trimethoprim Drug Dose on Corrosion Behavior of Stainless Steel in Simulated Human Body Environment: Experimental and Theoretical Investigations. *J Bio-Tribo-Corros.* 2021; 7(3): 8-13. <https://doi.org/10.1007/s40735-021-00559-8>
13. Fawzy A, Toghan A. Inhibition Evaluation of Chromotrope Dyes for the Corrosion of Mild Steel in an Acidic Environment: Thermodynamic and Kinetic Aspects. *ACS Omega.* 2021 Jan 25; 6(5): 4051-4061. <https://doi.org/10.1021/acsomega.0c06121>
14. Mustafa S R, Al-Ani H N. Calculation of vibrational frequencies, Energetic and some other Quantum Chemical Parameters for some Flavonoids, *J Phys Conf Ser.* 2021(1): 12018. <https://doi.org/10.1088/17426596/1999/1/012018>
15. Abdulridha MQ, Al-hamdani AAS, Hussein I A. Synthesis, Characterization and Antioxidant Activity of New Azo Ligand and Some Metal Complexes of Tryptamine Derivatives. *Baghdad Sci J.* 2023; 20: 1046-1063. <https://doi.org/10.21123/bsj.2023.8227>
16. Naser A W, Abdullah AFJ. Synthesis of some new N-saccharin derivatives of possible biological activity. *Chem Pharm Res.* 2014, 6(5): 872-879.
17. Mohammed HS, Al-Saadawy NH. Synthesis, Characterization and Theoretical Investigation of Innovative Charge-transfer Complexes Derived from the N-phenyl 3, 4-selenadiazole Benzophenone Imine. *Baghdad Sci J.* 2023; 20(5): 1943-1963. <https://doi.org/10.21123/bsj.2023.7748>
18. Dhumad AM, Hassan QM, Fahad TA, Emshary CA, Raheem NA, Sultan HA. Synthesis, structural characterization and optical nonlinear properties of two azo- β -diketones. *J. Mole .Struct.* 2021; 5 July,1235, 130196. <https://doi.org/10.1016/j.molstruc.2021.130196>
19. Kudelko A, Olesiejuk M, Luczynski M, Swiatkowski M, Sieranski T, Kruszynski R. 1,3,4-Thiadiazole-Containing Azo Dyes: Synthesis, Spectroscopic Properties and Molecular Structure. *Molecules.* 2020; 25(12): 2822-2839. <https://doi.org/10.3390/molecules25122822>
20. Ahmed M A, Jasdeep K, Akhil S, Mahmoud A B, Dakeshwar K V, Elyor B. Electrochemical and DFT studies of Terminalia bellerica fruit extract as an eco-friendly inhibitor for the corrosion of steel. *Nature.* 2023; 13(19367): 1-22. <https://doi.org/10.1038/s41598-023-45283-0>
21. Mahmoud AB, Hani ME, Ahmed B, Rabab MA, Abed El-ziz SF. Novel coumarin-buta-1,3-diene conjugated donor-acceptor systems as corrosion

- inhibitors for mild steel in 1.0 M HCl: Synthesis, electrochemical, computational and SRB biological resistivity. Sci Direct. 2023; 148(15): 128644 <https://doi.org/10.1016/j.inoche.2022.110304>.
22. Kubba, MR, Abood KF. DFT, PM3, AM1, and MINDO/3 Quantum Mechanical Calculations for Some INHC Cs Symmetry Schiff Bases as Corrosion Inhibitors for Mild Steel. Iraqi J Sci. 2023; 56(1C): 602–621. <https://doi.org/10.9734/bpi/mono/978-93-91882-61-7/CH5>.
23. Mahmoud A B, Hani M E, Ahmed H B, Rabab M A, Abed El-ziz S F. Novel coumarin-buta-1,3-diene conjugated donor–acceptor systems as corrosion inhibitors for mild steel in 1.0 M HCl: Synthesis, electrochemical, computational and SRB biological resistivity. Sci Direct. 2023; 148(15): 128644. <https://doi.org/10.1016/j.inoche.2022.110304>.
24. Kubba RM, Mohammed MA. Theoretical and Experimental Study of Corrosion Behavior of Carbon Steel Surface in 3.5% NaCl and 0.5 M HCl with Different Concentrations of Quinolin-2-One Derivative. Baghdad Sci J. 2022; 19(1): 105-120. <https://doi.org/10.21123/bsj.2022.19.1.0105>.
25. Ahmed AH, Kuba RM, Al-Majidi SMH. Synthesis, Identification, Theoretical and Experimental Studies of Carbon Steel Corrosion Inhibition in Sea Water by Some New Diazine Derivatives linked to 5-Nitro Isatin Moiety. Iraqi J Sci. 2018; 59(3B): 1347–1365. <https://doi.org/10.24996/ij.s.2018.59.3B.2>.
26. Khudhair NA, Bader AT, Ali MI, Hussein M. Synthesis, identification and experimental studies for carbon steel corrosion in hydrochloric acid solution for polyimide derivatives. AIP Conf Proc. 2020; 2290(1): 030014. <https://doi.org/10.1063/5.0027443>.

تحضير وتشخيص صبغتين مشتقتين من بارا-أمينو فينول ودراسة فعاليتهما كمثبطات للتآكل: التحليل التجريبي والنظري

اسيل فرحان عبد الله ، سرى حامد كاظم، عذراء كظامي صكر ، جواد كاظم عبيس

قسم الكيمياء ، كلية العلوم ، جامعة واسط ، الكوت ، العراق.

الخلاصة

تم في هذا البحث تحضير صبغتين من بارا-امينو فينول من خلال تفاعل ملح الديزونيوم من بارا-امينو فينول مع مركبين اروماتي (1-نفنول وبارا-امينو فينول). تم تشخيص الصبغتين الجديدتين (a و b) بتقنية FTIR و¹HNMR مع قياس بعض الخواص الفيزيائية. تم دراسة النشاط التثبيطي تجريبياً بواسطة القياسات الكهروكيميائية لمركبات الأزو المحضرة ضد تآكل الفولاذ الكربوني نوع C45 في وسط (0.1 M, HCl). تم استخدام طريقة ميكانيكا الكم لحساب البنية الهندسية والخواص الفيزيائية بواسطة برنامج Gaussian 09 ونظرية الكثافة الوظيفية (DFT) لدالة B3LYP بمستوى 6-311 G⁺(2d, 2p). تم استخدام نظرية الكثافة الوظيفية في حساب معاملات كفاءة التثبيط للصبغتين في وسط مفرغ من الهواء. وأظهرت النتائج ان المركب a الافضل بالتثبيط.

الكلمة المفتاحية: أزو، مثبط التآكل، نظرية الكثافة الوظيفية، الكيمياء الكهربائية، شحنات موليكين.